# Excitons in resonant tunnelling structures based on AlN/GaN/AlN/AlGaN/AlN nitride: spectral dependences and intensities of interband optical transitions

[1] Boyko I., [1] Petryk M. and [1, 2] Mykhailyshyn R.

[1] Ternopil Ivan Puluj National Technical University, 56 Ruska Street, 46001 Ternopil, Ukraine boyko.i.v.theory@gmail.com
[2] Department of Robotics Engineering, Worcester Polytechnic Institute, 85 Prescott Street, Worcester, Massachusetts, USA

**Received**: 27.05.2022

**Abstract.** We offer a new iterative method for exciton theory and develop a theory of exciton states arising in a plane resonant-tunnelling nanostructure based on semiconducting nitrides. Our approach takes into account the contributions of internal electric fields arising in its layers and employs both iterative and variational methods. We compare our method with the other techniques known in the exciton theory on example of a nanosystem representing a separate cascade of quantum cascade detector, which has been earlier implemented experimentally. The electron and hole spectra, the spectra of excitons and their binding energies, as well as the intensities of electron–hole transitions are calculated as functions of geometric parameters of the nanostructure. Particular cases of light-hole and heavy-hole excitons are analyzed.

**Keywords:** excitons, nitride semiconductors, quantum cascade detectors, resonant tunnelling structures, variational methods, iterative methods.

**UDC:** 538.958; 538.971

## 1. Introduction

Modern semiconductor optoelectronic devices such as quantum cascade lasers and quantum cascade detectors (QCDs) [1–3] are based on the quantum transitions that occur between the electronic states of plane resonant tunnelling semiconducting structures. Utilization of III- and IV-group nitrides is especially important when producing the QCDs operating in the near and middle infrared ranges. In spite of extensive experimental and theoretical studies of the electronic processes taking place in the nanostructures based on such semiconductors (e.g., AlN, GaN, AlGaN and InGaN), these processes are still not studied in sufficient detail. The same is true of the excitons themselves since the theory of the latter is far from completeness. In this respect one has to mention the influential works concerned with the excitons in nitrides. They have been aimed at the effect of displacement of energy bands [4], localization of excitons [5], their interaction with optical phonons [6] and temperature stability [7], and the effect of hydrostatic pressure on the exciton states [8]. The studies associated with geometric confinement for the exciton spectra have addressed mainly AlN/AlGaN quantum dots [9–11].

It is also known [12, 13] that the main factor affecting the electronic transitions in nitride-based nanostructures is the internal electric field determined by the total spontaneous and piezoelectric polarizations. This circumstance makes it impossible to apply directly a model of rectangular potential wells and barriers. The influence of this internal field has mainly been analyzed for quantum dots and single-well nanostructures [11, 14–16]. Multilayer GaN/AlGaN nanostructures have been addressed in the work [17]. However, the exciton states have been analyzed with no consideration of the

internal electric fields, which undermines both the theoretical and practical value of this study.

It is also worthwhile to mention the studies [18, 19] where exciton-binding energies have been calculated for the strained single- and double-well AlGaN/GaN nanostructures. On the one hand, the contribution of the internal electric field has indeed been taken into account there. On the other hand, the authors of the above works have pursued the goals somewhat different from our main subject. In particular, they have studied the effect of hydrostatic pressure on the exciton states. Finally, the nanosystems [18, 19] represent basic elements of resonant tunnelling diodes and waveguides, which are only partly adjacent to the QCDs.

Although the variational method represents a common contemporary technique in the exciton theory, its applicability to the nanostructures with strong internal electric fields has not yet been evaluated. This can be done after developing another calculation method (e.g., iterative one) and comparing the results obtained by the two methods. It is also worth noticing that the cases of light and heavy holes have not yet been studied and compared with each other for the nanostructures of the type mentioned above. In particular, this concerns the spectral parameters of holes, the exciton energies and the intensities of interband transitions. Solving of these theoretical problems is the immediate goal of the present work.

## 2. Exciton Hamiltonian. Spectra of non-interacting electron and hole

Below we will deal with the exciton states arising in a double-well AlN/GaN/AlN/AlGaN/AlN nanostructure, which operates as a separate cascade (see the experimental work [2]). A geometric scheme of the nanostructure and its energy schemes for electron and hole are illustrated in Fig. 1. Using the notation of Fig. 1, one can represent the effective mass of electron (or hole) as

$$\begin{aligned} m^{(\alpha)}(z_\alpha) &= m_0^{(\alpha)}\left\{\theta(-z_\alpha)+\theta(z_\alpha - z_\alpha^{(5)})+\sum_{p=0}^{2}\left[\theta(z_\alpha - z_\alpha^{(2p)})-\theta(z_\alpha - z_\alpha^{(2p+1)})\right]\right\} \\ &+m_1^{(\alpha)}\left[\theta(z_\alpha - z_\alpha^{(1)})-\theta(z_\alpha - z_\alpha^{(2)})\right]+m_2^{(\alpha)}\left[\theta(z_\alpha - z_\alpha^{(p-1)})-\theta(z_\alpha - z_\alpha^{(p)})\right], \\ &\alpha=\{e,h\},\ z_\alpha^{(0)}=0,\ z_\alpha^{(-1)}=-\infty,\ z_\alpha^{(6)}=+\infty. \end{aligned} \tag{1}$$

Here $m_0^{(\alpha)}$, $m_1^{(\alpha)}$ and $m_2^{(\alpha)}$ are the effective masses of electron (or hole) in the layers corresponding respectively to AlN (potential barriers), GaN and AlGaN (quantum wells), while $\theta(z)$ is the unit Heaviside step function.

The energies of the exciton and its wave functions can be obtained by finding the solutions of a stationary Schrödinger equation:

$$\hat{H}_{ex}(\rho, z_e, z_h)\Psi(\rho, z_e, z_h) = E_{ex}\Psi(\rho, z_e, z_h), \tag{2}$$

where $\rho$ denotes the relative distance between electron and hole in the $xOy$ plane, and $z_e$ and $z_h$ are the electron and hole coordinates on the $z$ axis. The exciton Hamiltonian is defined as follows:

$$\begin{aligned} \hat{H}_{ex}(\rho, z_e, z_h) &= E_g + \hat{H}^{(e)}(z_e) + \hat{H}^{(h)}(z_h) \\ &+\hat{H}_r(\rho, z_e, z_h) + V\left(\left|z_e - z_h\right|\right) \end{aligned}, \tag{3}$$

where $E_g$ is the bandgap, $\hat{H}^{(e)}(z_e)$ and $\hat{H}^{(h)}(z_h)$ are the Hamiltonians of free electron and hole, respectively, $\hat{H}_r(\rho, z_e, z_h)$ implies the Hamiltonian describing relative motion of electron and hole, and $V\left(\left|z_e - z_h\right|\right)$ refers to the Coulomb interaction of electron and hole.

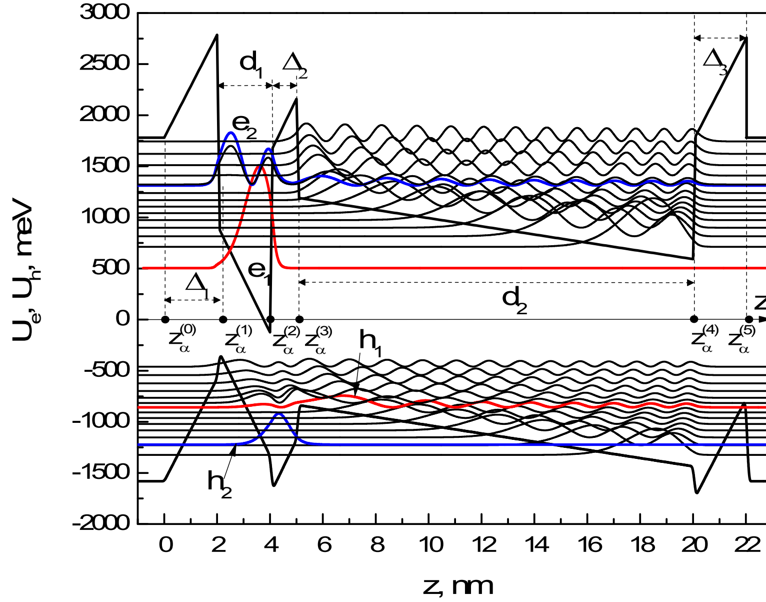


**Fig. 1.** A geometric scheme and energy schemes (for electron and hole) of a nanostructure under study: $z_\alpha$ specify coordinates of the boundaries between layers, dashed lines denote these boundaries, $d_1, d_2$ and $\Delta_1, \Delta_2, \Delta_3$ determine the sizes of respectively potential wells and potential barriers, and $e_1, e_2$ (or $h_1, h_2$) give the first two electron (or hole) states localized in the input potential well.

Let us now reveal the physical meaning of each of the terms in Eq. (3). The parameter

$$E_g = \begin{cases} E_g^{(\mathrm{GaN})}, \; z_\alpha^{(1)} \le z_\alpha \le z_\alpha^{(2)}, \\ E_g^{(\mathrm{AlGaN})}, \; z_\alpha^{(3)} \le z_\alpha \le z_\alpha^{(4)}, \\ E_g^{(\mathrm{AlN})}, \; z_\alpha < 0, \; 0 \le z_\alpha \le z_\alpha^{(1)}, z_\alpha^{(2)} \le z_\alpha \le z_\alpha^{(3)}, \; z_\alpha^{(4)} \le z_\alpha \le z_\alpha^{(5)}, z_\alpha > z_\alpha^{(5)} \end{cases} \tag{4}$$

represents the bandgap, the temperature dependence of which is calculated according to the Varshni relation [13]

$$E_g^{(\beta)}(T) = E_g^{(\beta)}(T)\Big|_{T=0} - \frac{a^{(\beta)} T^2}{b^{(\beta)} + T}, \quad . \\ \beta = \{\mathrm{AlN}, \; \mathrm{GaN}\} \tag{5}$$

In case of $\mathrm{Al}_x\,\mathrm{Ga}_{1-x}\mathrm{N}$ semiconductor, the dependence of the bandgap on the composition $x$ ($0 \le x \le 1$) can be calculated as

$$E_g(x) = xE_g^{(\mathrm{AlN})} + (1-x)E_g^{(\mathrm{GaN})} + cx(1-x) \,. \tag{6}$$

where $a$ and $b$ are the Varshni parameters which are different for different semiconductors and $c$ represents the bowing parameter [20].

The Hamiltonians for non-interacting electron and hole in Eq. (3) are defined as follows:

$$\hat{H}^{(\alpha)}(z_\alpha) = -\frac{\hbar^2}{2}\frac{\partial}{\partial z_\alpha}\frac{1}{m^{(\alpha)}(z_\alpha)}\frac{\partial}{\partial z_\alpha} + U^{(\alpha)}(z_\alpha) + U_E^{(\alpha)}(z_\alpha), \tag{7}$$

with $U^{(\alpha)}(z_\alpha)$ implying the effective potential for the nanostructure in which there is no interaction of electron and hole with the internal electric field. Namely, we have

$$U^{(e)}(z_e)=\begin{cases}0,\\ 0.765(E_g^{(\mathrm{AlGaN})}-E_g^{(\mathrm{GaN})}),\\ 0.765(E_g^{(\mathrm{AlN})}-E_g^{(\mathrm{GaN})}),\end{cases} U^{(h)}(z_h)=\begin{cases}0, \text{ in GaN well},\\ 0.235(E_g^{(\mathrm{AlGaN})}-E_g^{(\mathrm{GaN})}), \text{ in AlGaN well},\\ 0.235(E_g^{(\mathrm{AlN})}-E_g^{(\mathrm{GaN})}), \text{ in AlN barriers.}\end{cases} \quad (8)$$

The component $U_E^{(\alpha)}(z_\alpha)$ characterizing the contribution of the internal electric field is given by

$$U_E^{(\alpha)}(z_\alpha)=q^{(\alpha)}\sum_{p=1}^{5}(-1)^{p-1}(F_p z_\alpha - F_{p-1}z_\alpha^{(p-1)})\left[\theta(z_\alpha - z_\alpha^{(p-1)})-\theta(z_\alpha - z_\alpha^{(p)})\right],$$

$$F_0=0,\ q^{(\alpha)}=\begin{cases}q^{(e)}=-e,\\ q^{(h)}=e.\end{cases} \quad (9)$$

The electric field strength $F_p$ in Eq. (9) is determined by the contributions of total spontaneous ($P_{sp}^{(p)}$) and piezoelectric ($P_{pz}^{(p)}$) polarizations. The direct calculations can be performed using the continuity condition for the electric induction $\bar{D}_p=\varepsilon^{(p)}\bar{F}_p+\bar{P}_p$ at all internal surfaces of the nanostructure:

$$D_p = D_{p+1},\ p=0..5\ . \quad (10)$$

Besides, one has to take into account the condition for the total voltage drop across the nanostructure [13]:

$$\sum_{p=1}^{5}F_p\left(z_\alpha^{(p-1)}-z_\alpha^{(p)}\right)=0\ . \quad (11)$$

Having solved the system of Eqs. (10) and (11), we obtain the electric field in a separate layer of our nanostructure with the thickness $z_\alpha^{(p-1)}-z_\alpha^{(p)}$:

$$F_p=\frac{1}{\varepsilon_{(p)}^{(\alpha)}}\sum_{\substack{k=1\\k\neq p}}^{5}\frac{\left[\left(P_{sp}^{(k)}+P_{pz}^{(k)}\right)-\left(P_{sp}^{(p)}+P_{pz}^{(p)}\right)\right]\left(z_\alpha^{(p-1)}-z_\alpha^{(p)}\right)}{\varepsilon_{(k)}^{(\alpha)}}\Bigg/\sum_{k=1}^{5}\frac{z_\alpha^{(k-1)}-z_\alpha^{(k)}}{\varepsilon_{(k)}^{(\alpha)}}\ . \quad (12)$$

Here summation over the index *k* is carried out, whereas $\varepsilon_{(p)}^{(\alpha)}$ (or $\varepsilon_{(k)}^{(\alpha)}$) denotes the dielectric permittivity of the *p*-th (or *k*-th) layer of the nanostructure. In general, we have the relation

$$\varepsilon^{(\alpha)}(z_\alpha)=\varepsilon_0^{(\alpha)}\left\{\theta(-z_\alpha)+\theta(z_\alpha-z_\alpha^{(5)})+\sum_{p=0}^{2}\left[\theta(z_\alpha-z_\alpha^{(2p)})-\theta(z_\alpha-z_\alpha^{(2p+1)})\right]\right\}$$
$$+\varepsilon_1^{(\alpha)}\left[\theta(z_\alpha-z_\alpha^{(1)})-\theta(z_\alpha-z_\alpha^{(2)})\right]+\varepsilon_2^{(\alpha)}\left[\theta(z_\alpha-z_\alpha^{(p-1)})-\theta(z_\alpha-z_\alpha^{(p)})\right], \quad (13)$$

where $\varepsilon_0^{(\alpha)}$, $\varepsilon_1^{(\alpha)}$ and $\varepsilon_2^{(\alpha)}$ are the dielectric constants of the nanostructure layers corresponding respectively to AlN, GaN and AlGaN semiconductors.

The relative motion of electron and hole in the coordinate system reduced to their centre of mass is determined by the Hamiltonian component given by Eq. (3):

$$\hat{H}_r(\rho,z_e,z_h)=-\frac{\hbar^2}{2\mu(z_e,z_h)}\left(\frac{\partial^2}{\partial\rho^2}+\frac{1}{\rho}\frac{\partial}{\partial\rho}\right), \quad (14)$$

with

$$\mu(z_e,z_h)=\frac{m^{(e)}(z_e)m^{(h)}(z_h)}{m^{(e)}(z_e)+m^{(h)}(z_h)} \quad (15)$$

being the reduced exciton mass. The component of the Hamiltonian (3) defining the potential energy of interaction between electron and hole reads as

$$V(|z_e - z_h|) = -\frac{e^2}{\varepsilon(z_e, z_h)\sqrt{\rho^2 + (z_e - z_h)^2}}, \ \varepsilon(z_e, z_h) = \varepsilon^{(e)}(z_e) = \varepsilon^{(h)}(z_e). \quad (16)$$

The spectra of free electron and hole are obtained by finding the solutions of the stationary Schrödinger equation:

$$\left[-\frac{\hbar^2}{2}\frac{\partial}{\partial z_\alpha}\frac{1}{m^{(\alpha)}(z_\alpha)}\frac{\partial}{\partial z_\alpha} + U^{(\alpha)}(z_\alpha) + U_E^{(\alpha)}(z_\alpha)\right]\Psi^{(\alpha)}(z_\alpha) = E^{(\alpha)}\Psi^{(\alpha)}(z_\alpha). \quad (17)$$

This gives

$$\begin{aligned} &\Psi^{(\alpha)}(z_\alpha) = A_{(0)}^\alpha e^{\chi_{(0)}^\alpha z_\alpha}\theta(-z_\alpha) + B_{(6)}^\alpha e^{-\chi_{(6)}^\alpha z_\alpha}\theta(z_\alpha - z_\alpha^{(5)}) \\ &+\sum_{p=1}^{5}\left\{A_{(p)}^\alpha Ai\left[\zeta_{(p)}^\alpha(z_\alpha)\right] + B_{(p)}^\alpha Bi\left[\zeta_{(p)}^\alpha(z_\alpha)\right]\right\}\left[\theta(z_\alpha - z_\alpha^{(p-1)}) - \theta(z_\alpha - z_\alpha^{(p)})\right], \\ &\zeta_{(p)}^\alpha(z_\alpha) = \left(2m_0^{(\alpha)}q^{(\alpha)}F_p/\hbar^2\right)^{1/3}\left[(U^{(\alpha)}(z_\alpha) - E)/q^{(\alpha)}F_p - z_\alpha\right], \\ &\chi_{(0)}^\alpha = \chi_{(6)}^\alpha = \hbar^{-1}\sqrt{2m_0^{(\alpha)}(U^{(\alpha)}(z_\alpha)\big|_{z_\alpha<0,\ z_\alpha>z_\alpha^{(5)}} - E)}, \end{aligned} \quad (18)$$

where $Ai(z)$ and $Bi(z)$ are the Airy functions, and $A_{(p)}^\alpha$ and $B_{(p)}^\alpha$ denote the coefficients appearing in the solutions of Eq. (17) for the $p$-th layer of the nanostructure. The dispersion equation defining the electron and hole spectra ($E_n^\alpha$) can be found from the boundary conditions that describe continuity of the wave function of electron (hole) and a flow of its probability density (calculated as $J = i\hbar\left(\Psi_{(p)}^\alpha d\Psi^{*\alpha}_{(p)}/dz - \Psi^{*\alpha}_{(p)}d\Psi_{(p)}^\alpha/dz\right)/2m^{(\alpha)}(z)$) through all heteroboundaries of the nanosystem:

$$\Psi_{(p)}^\alpha(E, z_\alpha^{(p)}) = \Psi_{(p+1)}^\alpha(E, z_\alpha^{(p)}); \ \left.\frac{d\Psi_{(p)}^\alpha(E, z_\alpha)}{m^{(\alpha)}(z_\alpha)dz_\alpha}\right|_{z=z_\alpha^{(p)}-\varepsilon} = \left.\frac{d\Psi_{(p+1)}^\alpha(E, z_\alpha)}{m^{(\alpha)}(z_\alpha)dz_\alpha}\right|_{z=z_\alpha^{(p)}+\varepsilon}, \ \varepsilon \to 0. \quad (19)$$

In addition, the boundary conditions given by Eq. (19) enable one to express sequentially all the coefficients $A_{(0)}^\alpha$, $B_{(6)}^\alpha$, $A_{(p)}^\alpha$ and $B_{(0)}^\alpha$ in terms of one coefficient taken arbitrarily from their set. To find this coefficient, we use normalization condition for the wave function:

$$\int_{-\infty}^{+\infty}\Psi_n^{(\alpha)*}(E_n^\alpha, z_\alpha)\Psi_{n'}^{(\alpha)}(E_{n'}^\alpha, z_\alpha)dz = \delta_{nn'}, \quad (20)$$

with $\delta_{nn'}$ being the Kronecker delta. In this manner, the wave functions of free electron and hole are completely defined.

## 3. Variational method

In general case, the solution of Eq. (2) with the Hamiltonian (3) cannot be obtained analytically, since the component (16) of the Hamiltonian describing the Coulomb interaction of electron and hole is too complicated. In order to calculate the exciton-binding energy, we represent the exciton wave function as a trial function [14]:

$$\Psi(\rho, z_e, z_h) = \Psi^{(e)}(z_e)\Psi^{(h)}(z_h)\Phi(\rho), \quad (21)$$

where the functions $\Phi(\rho)$ are chosen similarly to the functions for a hydrogen-like atom:

$$\Phi(\rho)=\sqrt{\frac{2}{\pi\lambda^2}}e^{-\rho/\lambda}\,. \tag{22}$$

Here $\lambda$ represents a variational parameter, on which the binding energy of the exciton now depends. In its turn, the binding energy of the exciton in its ground state is determined from the minimization condition for the functional

$$E_{ex}=\min_{\lambda}\frac{\left\langle \Psi^{(e)}(z_e)\Psi^{(h)}(z_h)\Phi(\rho)\middle|\hat{H}_{ex}(\rho,z_e,z_h)\middle|\Psi^{(e)}(z_e)\Psi^{(h)}(z_h)\Phi(\rho)\right\rangle}{\left\langle \Psi^{(e)}(z_e)\Psi^{(h)}(z_h)\Phi(\rho)\middle|\Psi^{(e)}(z_e)\Psi^{(h)}(z_h)\Phi(\rho)\right\rangle}\,. \tag{23}$$

It can be seen from Eqs. (3) and (23) that the binding energy $E_b$ of exciton and the energy $E_{ph}$ of electron–hole transition can be defined respectively as

$$E_b=E^{(e)}+E^{(h)}-E_{ex};\; E_{ph}=E_g-E_{ex}\,. \tag{24}$$

Using the wave functions of electron and hole, one can calculate the intensities of the interband transitions:

$$I_{n_e n_h}=\left|\int_{-\infty}^{+\infty}\Psi^{(e)}(z)\Psi^{(h)}(z)dz\right|^2 . \tag{25}$$

## 4. Iterative method

A presence of strong electric field given by Eq. (12) complicates significantly the calculations aimed at minimizing the functional (23). To overcome this problem, we will use an iterative method based on the idea suggested in Ref. [21], where the effect of magnetic field on the exciton states in InGaAs quantum well has been studied.

Substituting Eqs. (21) and (22) into Eq. (23) and minimizing the last expression with respect to the parameter $\lambda$ in a standard way, we obtain

$$E_{ex}=4e^2\min_{\lambda}\left\{\int_{-\infty}^{+\infty}\frac{\left|\Psi^{(e)}(z_e)\right|^2}{\varepsilon(z_e,z_h)}\int_{-\infty}^{+\infty}\left|\Psi^{(h)}(z_h)\right|^2\int_0^{+\infty}\frac{\rho\exp(-2\rho/\lambda)d\rho dz_e dz_h}{\sqrt{\rho^2+(z_e-z_h)^2}}-\frac{\hbar^2}{2\mu\lambda^2}\right\}, \tag{26}$$

with $\mu=\mu(z_e,z_h)$. Now the immediate problem is to calculate this integral. The electronic and hole functions given by Eq. (18), which contain the Airy functions, complicate significantly the calculations in terms of computation time, especially the calculations performed for multilayer nanosystems.

Next we will adopt two approximations. First, let us approximate the wave functions in the nanostructure as

$$\begin{gathered}\Psi_\alpha^{(\alpha)}(z_\alpha)=A_{(p)}^{\alpha}Ai\left[\zeta_{(p)}^{\alpha}(z_\alpha)\right]+B_{(p)}^{\alpha}Bi\left[\zeta_{(p)}^{\alpha}(z_\alpha)\right]\approx\widetilde{\Psi}_\alpha^{(\alpha)}(z_\alpha)\\ =\sum_{i=1}^{N}\left(\widetilde{A}_{(p_s)}^{\alpha}e^{ik_\alpha^{(pl)}z_\alpha}+\widetilde{B}_{(p)}^{\alpha}e^{-ik_\alpha^{(pl)}z_\alpha}\right)\left[\theta\left(z-z_\alpha^{p_l}\right)-\theta\left(z-z_\alpha^{p_{l+1}}\right)\right],\; k_\alpha^{(p_l)}=\sqrt{2m_\alpha^{(p_l)}(U^{(\alpha)}(z_\alpha)-E)}\Big/\hbar\,,\end{gathered} \tag{27}$$

where $m_\alpha^{(p_l)}$ is the effective mass of electron (or hole) in a different segment of our nanosystem. Such an approximation in fact separates the area of any nanostructure layer into segments by the points $z_\alpha^{p_l}=l\left(z_\alpha^{(p)}-z_\alpha^{(p-1)}\right)\big/2N$. Below we put $N=10$ in our calculations. We assume that, inside

each of the resulting segments, the boundary conditions similar to those given by Eq. (19) are satisfied. Then the condition (23) yields the expression for the exciton binding energy:

$$E_{ex}=\frac{4e^2}{\varepsilon^{(\alpha)}(z_\alpha)}\min_\lambda\left\{\left(\int_{-\infty}^{+\infty}\left|\widetilde{\Psi}_\alpha^{(\alpha)}(z_\alpha)\right|^2dz_e\right)\left(\int_{-\infty}^{+\infty}\left|\widetilde{\Psi}_\alpha^{(\alpha)}(z_\alpha)\right|^2dz_h\right)\int_0^{+\infty}\frac{\rho\exp(-2\rho/\lambda)d\rho}{\sqrt{\rho^2+(z_e-z_h)^2}}-\frac{\hbar^2}{2\mu\lambda^2}\right\}, \quad (28)$$

where the relation $\varepsilon(z_e,z_h)=\varepsilon^{(\alpha)}(z_\alpha)$ is assumed. Now we expand the function involved in Eq. (28) in a Taylor series

$$1\Big/\sqrt{1+[(z_e-z_h)/\rho]^2}=\rho/(z_e-z_h)-\rho^3\big/2(z_e-z_h)^3+3\rho^5\big/8(z_e-z_h)^5-5\rho^7\big/16(z_e-z_h)^7+\dots .$$

Then the integral can be approximated by

$$\int_0^{+\infty}\frac{\exp(-2\rho/\lambda)d\rho}{\sqrt{1+[(z_e-z_h)/\rho]^2}}=\frac{\lambda^2}{4(z_e-z_h)}-\frac{3\lambda^4}{16(z_e-z_h)^3}+\frac{45\lambda^6}{64(z_e-z_h)^5}-\frac{1575\lambda^8}{64(z_e-z_h)^7}+\dots \quad (29)$$

The above procedure simplifies greatly the calculations according to Eq. (28) and facilitates their practical implementation. The appropriate accuracy is given by the number $S$ of terms in the series (29) and the number $N$ of divisions of the layers in our nanosystem into separate segments.

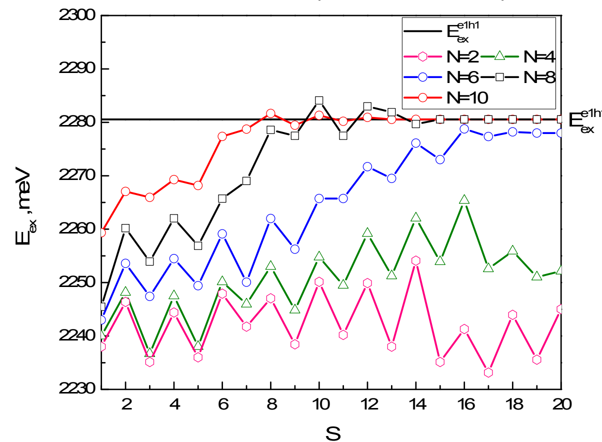


**Fig. 2.** Illustration of convergence of our iterative procedure for calculating the exciton energy $E_{ex}^{e1h1}$ as a function of number $N$ of segments of the layers and number $S$ of iterations.

Fig. 2 shows dependences of the calculated exciton energies on the $S$ parameter for different partitions given by the $N$ number. A black horizontal line in Fig. 2 indicates the light-exciton energy obtained by direct numerical calculations. At $N = 2$ and $N = 4$, increase in the number of terms in Eq. (29) in the region $1 \le S \le 20$ does not lead to convergence of the iterative procedure. The iterative process converges at $N = 6$, although the final exciton energy is slightly less than the corresponding value calculated numerically. Finally, the iterative procedure clearly converges to the latter value at $N = 8$ and $N = 10$. As mentioned above, we put $N = 10$ in our calculations to ensure a sufficient accuracy and coordinate the convergence of the calculations performed in frame of the both schemes.

## 5. Discussion of results

The electron and hole spectra and the exciton-binding energy have been calculated using the theory presented above. To be specific, we have used the parameters associated with a separate cascade in a QCD, which has been studied both experimentally [2] and theoretically [20]. Our

choice is easily understood since the main aspects of self-consistent calculations of the potential profiles for this structure have been already analyzed in the literature. Moreover, our choice of nanostructure is justified by its optimal geometric configuration. In fact, a separate QCD cascade under study represents a double-well resonant tunnelling structure. The geometric parameters of the above experimental nanostructure are as follows: $d_1^{\exp} = 2.08$ nm and $d_2^{\exp} = 2.08$ nm for the potential wells and $\Delta_1^{\exp} = 2.0$ nm, $\Delta_2^{\exp} = 1.0$ nm and $\Delta_2^{\exp} = 2.0$ nm for the potential barriers. The effective electron masses in GaN and AlN are equal to $m_e^{\mathrm{GaN}} = 0.186\ m_e$ and $m_e^{\mathrm{AlN}} = 0.382\ m_e$, while the effective masses of light and heavy holes are respectively $m_{lh}^{\mathrm{GaN}} = 0.153,\ m_e,\ m_{lh}^{\mathrm{AlN}} = 0.352\ m_e$ and $m_{hh}^{\mathrm{GaN}} = 1.400\ m_e,\ m_{hh}^{\mathrm{AlN}} = 3.530\ m_e$. These parameters have been adopted from the work [21].

Fig. 1 shows the potential profiles of our resonant tunnelling structure calculated for electron and hole with consideration of the internal electric field in the layers. According to Eqs. (9) and (12), the internal electric field deforms the energy scheme of the nanosystem both for electron and hole. In other words, it is the internal electric field that represents a principal factor influencing the spectra of these quasi-particles, thus causing subsidence of their discrete levels. The calculated squared wave functions for the electronic and hole states demonstrate clearly their localization in the nanostructure. They are reduced to the energy values for these levels. Special attention should be paid to the energy levels corresponding to red and blue lines in Fig. 1. The appropriate states are localized in the input active potential well of the resonant tunnelling structure, i.e. we deal with the working electron levels of the QCD implemented experimentally in the work [2].

Fig. 3 shows the calculated electronic spectrum and the spectra for light and heavy holes. These calculations have been carried out for the fixed parameters of potential barriers of the cascade so that the width of the input well $d_1$ changes from 0 to $d_1^{\exp} + d_2^{\exp}$ and the output well changes from $d_1^{\exp} + d_2^{\exp}$ to zero. In this case, the $d_1$ value specifies the relative position of the internal potential barrier in the total potential well of the cascade. The calculated spectra are presented in such a way that the electronic spectrum is measured from the bottom of the conduction band and the hole spectrum from the top of the valence band.

As seen from Fig. 3a, the levels of the electronic spectrum as functions of $d_1$ are formed at the value $d_1 = 0$. As $d_1$ increases, the levels are shifted to the low-energy region. One can observe anti-crossings of the energy levels due to tunnelling of electrons through the internal potential barrier. Note that the shift to the low-energy region is more pronounced for lower electronic levels, and the most rapid drop in these energies occurs when electron is localized in the input potential well with the probability close to unity. It is also a worthwhile fact that the anti-crossings seen in the spectra are the most significant for electron (Fig. 3a) and heavy hole (Fig. 3c). In general, the dependences of the spectra for light and heavy holes on the $d_1$ parameter are similar; however, it is seen from Fig. 3b, c that the heavy-hole spectrum includes a larger number of energy levels.

Next, we investigate the properties of intersubband transitions among the electron and hole states, which are localized in the active quantum well of the nanostructure. Notice that these energy levels are represented by the red and blue lines in Fig. 1 and indicated respectively as $e_1$, $e_2$ and $h_1$, $h_2$. The same notation is used for the dependences in Fig. 3. The importance of this subject is due to localization of these states and the fact that, for these transitions, it would be convenient to compare the intensities of electron–hole transitions for the two cases of light and heavy holes. The dependences of the intensity of interband transitions on $d_1$ are displayed in Fig. 4.

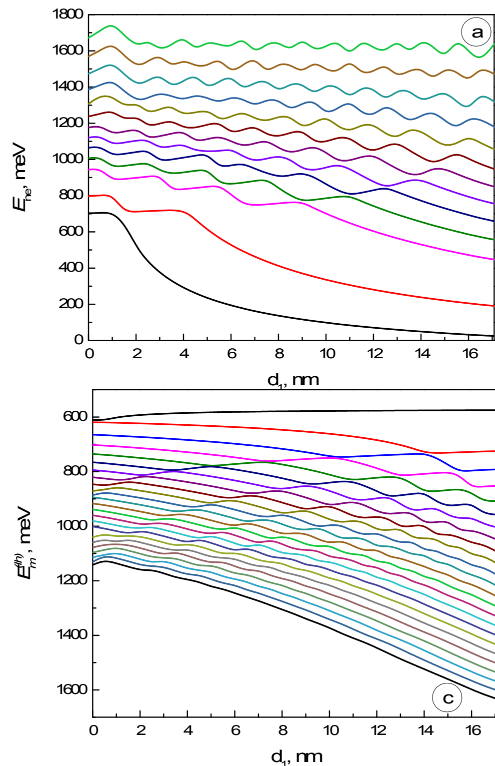


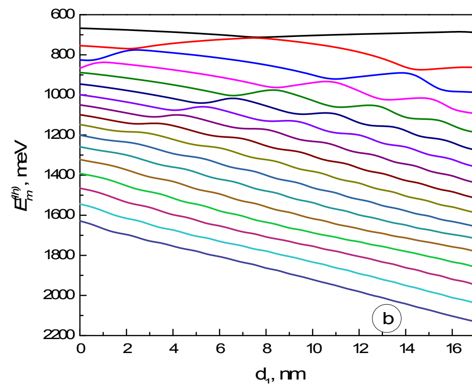


**Fig. 3.** Spectra calculated for electron (a) and for light (b) and heavy (c) holes as functions of $d_1$.

As seen from the dependences $I_{e_n h_n}(d_1)$ in Fig. 4a, b, the intensities of intersubband transitions between electron and light (see Fig. 4a) or heavy (see Fig. 4b) holes have a number of common features and differences. In the both dependences, there is a $d_1$ interval (10.2 nm < $d_1$ < 14.3 nm) where the condition $I_{e_1 h_1} >> I_{e_1 h_2}, I_{e_2 h_1}, I_{e_2 h_2}$ is satisfied. Moreover, the behaviours of the dependences $I_{e_n h_n}(d_1)$ for the light and heavy holes at $d_1$ > 14.3 nm are, in fact, identical. Invariable positions of narrow maximums occurring in the dependences $I_{e_1 h_1}(d_1)$ and $I_{e_2 h_1}(d_1)$ (located respectively at $d_1 \approx 1.79$ nm and $d_1 \approx 15.45$ nm ) must be mentioned in this respect.

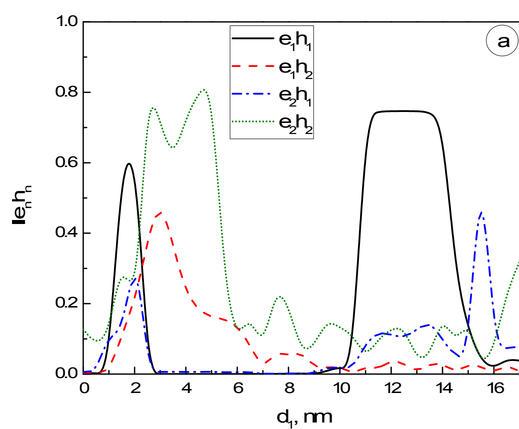


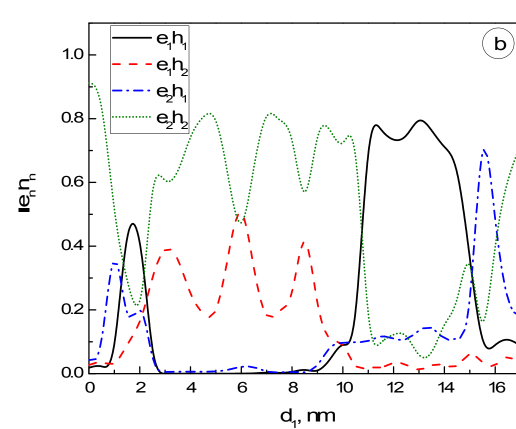


**Fig. 4.** Dependences of intersubband quantum transitions between electron–hole states $e_1h_1$, $e_1h_2$, $e_2h_1$ and $e_2h_2$ on $d_1$, as calculated for light (a) and heavy (b) holes.

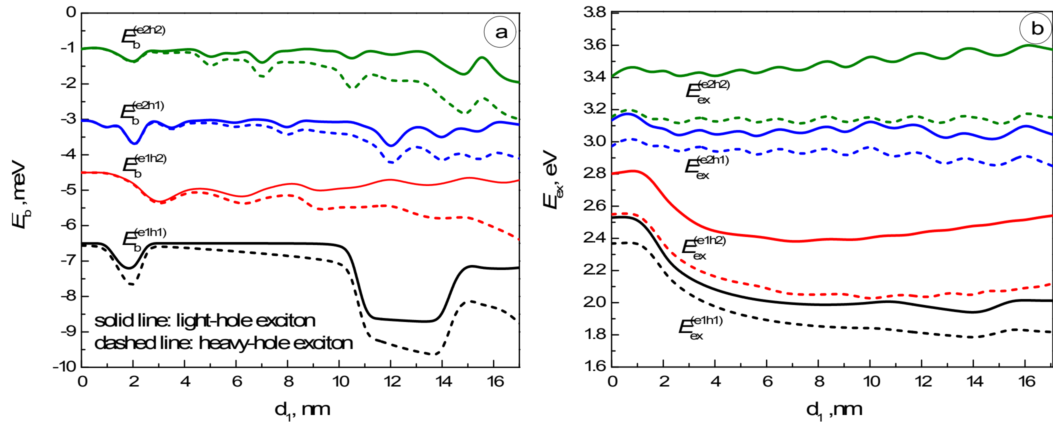


**Fig. 5.** Dependences of exciton-binding energies $E_b$ (a) and exciton energies $E_{ex}$ (b) on $d_1$, as calculated for the light-hole (solid lines) and heavy-hole (dashed lines) excitons.

Besides, in the case of heavy holes, the intensities $I_{e_2h_2}$ corresponding to the $d_1$ values close to zero exceed significantly the intensities for the other transitions. As seen from Fig. 4a, the intensity of intersubband transitions for the heavy holes inside the region 6.0 nm < $d_1$ < 11.0 nm is determined by the transitions $e_2 \to h_2$ and $e_1 \to h_2$. Note that this effect for the light holes seems to be not convincing.

The dependences of the calculated exciton-binding and exciton energies on $d_1$ are shown in Fig. 5. Here the calculations have been performed for the both light-hole and heavy-hole excitons in order to elucidate the differences in the properties of these excitons. As seen from Fig. 5a, the dependences of the binding energies for the light-hole and heavy-hole excitons on $d_1$ are similar and the energies acquire only negative values for all $d_1$'s. The absolute values of the binding energies are the largest for the exciton corresponding to the first electron and hole states, which are localized in the quantum well of the active zone. They are the smallest for the exciton formed by the second electron and hole states. Moreover, Fig. 5a testifies that a set of minima appears in the dependences, which is more pronounced in the case of $E_b^{e1h1}(d_1)$. For the other dependences, such minima are located in the region $1 \text{ nm} < d_1 < 4 \text{ nm}$ .

Note that the binding energy for the heavy-hole exciton manifests stronger dependence on $d_1$ than that of the light-hole exciton. Moreover, one can observe the effect of decrease in the binding energy with increasing $d_1$ for the heavy-hole exciton, which is not typical for the case of light-hole exciton. A number of important conclusions can be drawn from the data of Fig. 5b for the exciton spectra. The dependences $E_{ex}^{e1h1}(d_1)$ for heavy- and light-hole excitons and the dependence $E_{ex}^{e1h2}(d_1)$ for heavy-hole exciton are close to each other, and the same can be said of the dependences $E_{ex}^{e2h1}(d_1)$ for heavy- and light-hole excitons and the dependence $E_{ex}^{e2h2}(d_1)$ for heavy-hole exciton. Besides, the dependences $E_{ex}^{e1h2}(d_1)$ and $E_{ex}^{e2h2}(d_1)$ for the light-hole exciton differ significantly in the energy values from the other dependences formed by electron–hole pairs of the same states.

## 6. Conclusion

We suggest the quantum theory of the exciton states arising in the resonant tunnelling structures based on the group-III and group-IV nitride semiconductors. This theory has been developed using the two different approaches, variational and iterative ones. They are based on the approximation

of effective potential for the nanostructure under analysis. It has been found that our iterative procedure is convergent and its application is just as efficient as the variational method. Direct application of the two different approaches, variational and iterative, enable one to compare the limits of applicability of the both methods and find the conditions that provide quantitatively identical results of the two approaches.

Basing on the above methods and adopting the parameters from the experimentally functioning QCD, we have calculated the exciton spectra, the exciton-binding energies and the intensities of the electron–hole transitions. The results of our calculations are analyzed and compared for the cases of light-hole and heavy-hole excitons.

## References


1. Wang K, Grange T, Lin T, Wang L, Jehn Z, Birner S, Yun J, Terashima W and Hirayama H, 2018. Broadening mechanisms and self-consistent gain calculations for GaN quantum cascade laser structures. Appl. Phys. Lett. **113**: 061109.
2. Sakr S, Giraud E, Tchernycheva M, Isac N, Quach P, Warde E, Grandjean N and Julien F H, 2012. A simplified GaN/AlGaN quantum cascade detector with an alloy extractor. Appl. Phys. Lett. **101**: 251101.
3. Pesach A, Sakr S, Giraud E, Sorias O, Gal L, Tchernycheva M, Orenstein M, Grandjean N, Julien F H and Bahir G, 2014. First demonstration of plasmonic GaN quantum cascade detectors with enhanced efficiency at normal incidence. Opt. Express. **22**: 21069–21078.
4. Westmeyer A N, Mahajan S, Bajaj K K, Lin J Y and Jiang H X, 2006. Determination of energy-band offsets between GaN and AlN using excitonic luminescence transition in AlGaN alloys. J. Appl. Phys. **99**: 013705.
5. Ajia I A, Edwards P R, Liu Z, Yan J C, Martin R W and Roqan I S, 2014. Excitonic localization in AlN-rich $Al_xGa_{1-x}N/Al_yGa_{1-y}N$ multi-quantum-well grain boundaries. Appl. Phys. Lett. **105**: 122111.
6. Smith M, Lin J Y, Jiang H X, Khan A and Chen Q, 1997. Exciton-phonon interaction in InGaN/GaN and GaN/AlGaN multiple quantum wells. Appl. Phys. Lett. **70**: 2882–2884.
7. Bayerl D and Kioupakis E, 2019. Room-temperature stability of excitons and transverse-electric polarized deep-ultraviolet luminescence in atomically thin GaN quantum wells. Appl. Phys. Lett. **115**: 131101.
8. Staszczak G, Trzeciakowski W, Monroy E, Bercha A, Muzioł G, Skierbiszewski C, Perlin P and Suski T, 2020. Room-temperature stability of excitons and transverse-electric polarized deep-ultraviolet luminescence in atomically thin GaN quantum wells. Phys. Rev. B. **101**: 085306.
9. Fonoberov V A and Balandin A A., 2003. Excitonic properties of strained wurtzite and zinc-blende $GaN/Al_xGa_{1-x}N$ quantum dots. J. Appl. Phys. **94**: 7178–7186.
10. Williams D P, Andreev A D and O’Reilly P, 2006. Dependence of exciton energy on dot size in GaN/AlN quantum dots. Phys. Rev. B. **73**: R241301(R).
11. Chafai A, Essaoudi I, Ainane A, Dujardin F and Ahuja R, 2019. Binding energy of an exciton in a GaN/AlN nanodot: Role of size and external electric field. Physica B. **559**: 23–28.
12. Bernardini F and Fiorentini V, 2008. Macroscopic polarization and band offsets at nitride heterojunctions. Phys. Rev. B. **57**: R9427–R9430.
13. Boyko I V, 2018. Analytical method for calculation of the potential profiles of nitride-based resonance tunneling structures. Condens. Matter Phys. **21**: 43701.

14. Duque C M, Mora-Ramos M E and Duque C A, 2012. Exciton properties in zincblende InGaN-GaN quantum wells under the effects of intense laser fields. Nanoscale Res. Lett. **7**: 492.
15. Pokatilov E P, Nika D, Fomin V M and Devreese J T, 2008. Excitons in wurtzite AlGaN/GaN quantum-well heterostructures. Phys. Rev. B. **77**: 125328.
16. Wang H, Farias G A and Freire V N, 1999 Electric field effects on the confinement properties of GaN/$Al_xGa_{1-x}N$ zincblende and wurtzite nonabrupt quantum wells. Braz. J. Phys. **29**: 670–674.
17. Rojas-Briseno J G, Rodriguez-Vargas I, Mora-Ramos M E and Martinez-Orozco J C, 2020. Heavy and light exciton states in c-AlGaN/GaN asymmetric double quantum wells. Physica E. **124**: 114248.
18. Ha S H and Ban S L, 2008. Binding energies of excitons in a strained wurtzite GaN/AlGaN quantum well influenced by screening and hydrostatic pressure. Phys. Stat. Solidi B. **248**: 384–388.
19. Zhu J, BanS L and Ha S H, 2010. Binding energies of excitons in strained [0001]-oriented wurtzite AlGaN/GaN double quantum wells. J. Phys.: Condens. Matter. **20**: 085218.
20. Boyko I, 2018. Anisotropic wurtzite resonance tunneling structures: stationary spectrum of electron and oscillator strengths of quantum transitions. J. Phys. Stud. **22**: 1701.
21. Stepnicki P, Pietka B, Morier-Genoud F, Deveaud B and Matuszewski M, 2015. Analytical method for determining quantum well exciton properties in a magnetic field. Phys. Rev. B. **91**: 195302.
22. Vurgaftman I, Meyer J R and Ram-Mohan L R, 2001. Band parameters for III–V compound semiconductors and their alloys. J. Appl. Phys. **89**: 5815–5875.



Boyko I., Petryk M. and Mykhailyshyn R. 2022 Excitons in resonant tunnelling structures based on AlN/GaN/AlN/AlGaN/AlN nitride: spectral dependences and intensities of interband optical transitions. Ukr.J.Phys.Opt. **23**: 180 – 191. doi: 10.3116/16091833/23/3/180/2022



***Анотація***. *Запропоновано новий ітераційний метод для теорії екситонів і розвинуто теорію екситонних станів, які з'являються в плоскій резонансно-тунельній наноструктурі на основі напівпровідникових нітридів. Наш підхід враховує внески внутрішніх електричних полів, що виникають у шарах наноструктури. Він використовує і ітераційні, і варіаційні методи. Ми порівнюємо наш метод з іншими методами, відомими в теорії екситонів, на прикладі наносистеми, що представляє собою окремий каскад квантового каскадного детектора, який раніше був реалізований експериментально. Розраховано електронні та діркові спектри, спектри екситонів та енергії їхнього зв'язку, а також інтенсивності електронно-діркових переходів як функції геометричних параметрів наноструктури. Проаналізовано окремі випадки екситонів легких і важких дірок.*